

Parametric Resonance in Oscillations of Atmospheric Neutrinos?

Q.Y. Liu¹⁾, S.P. Mikheyev^{2,4)}, A.Yu. Smirnov^{3,4)} *

1) *Scuola Internazionale Superiore di Studi Avanzati, I-34013 Trieste, Italy*

2) *Laboratory Nazionale del Gran Sasso dell'INFN, I-67010 Assergi (L'Aquila), Italy*

3) *Abdus Salam International Centre for Theoretical Physics, I-34100 Trieste, Italy*

4) *Institute for Nuclear Research, Russian Academy of Sciences, 107370 Moscow, Russia*

Abstract

We consider a solution of the atmospheric neutrino problem based on oscillations of muon neutrinos to sterile neutrinos: $\nu_\mu \leftrightarrow \nu_s$. The zenith angle (Θ) dependences of the neutrino and upward-going muon fluxes in presence of these oscillations are studied. The dependences have characteristic form with two dips: at $\cos \Theta = -0.6 \div -0.2$ and $\cos \Theta = -1.0 \div -0.8$. The latter dip is due to parametric resonance in oscillations of neutrinos which cross the core of the earth. A comparison of predictions with data from the MACRO, Baksan and Super-Kamiokande experiments is given.

*e-mail addresses: qyliu@sissa.it, Stanislav@lngs.infn.it, Smirnov@ictp.trieste.it.

1. Introduction

Recently, the Super-Kamiokande [1] and Soudan [2] experiments have further confirmed an existence of the atmospheric neutrino problem [3,4]. Moreover, observations of the zenith angle as well as L/E (distance/energy) dependences of the muon neutrino deficit strongly indicate an oscillation solution of the problem.

Oscillations should give an observable effect in the zenith angle (Θ -)dependence of the flux of the upward-going muons produced by high energy neutrinos. However, the experimental situation is not yet clear. A peculiar Θ -dependence has been observed by MACRO experiment [5]. The ratio of the observed and expected fluxes as the function of Θ has two dips. The wide dip is in the range $\cos \Theta = -0.6 \div -0.2$ with minimum at $\cos \Theta = -0.4 \div -0.5$, and the narrow dip is at $\cos \Theta = -1.0 \div -0.8$ (vertical bins). In the narrow dip the observed flux is almost two times smaller than the expected one. Between these two dips ($\cos \Theta \sim -0.8$) the flux is close to the value without oscillations. It is important that for the vertical bins there is the best understanding of the acceptance and efficiencies. The probability of the no oscillation hypothesis is smaller than 1%, and inclusion of $\nu_\mu \rightarrow \nu_\tau$ oscillations does not raise the probability in a significant way [5]. Baksan experiment [6] has similar threshold for muon detection. The data also show a wide dip at $\cos \Theta = -0.6 \div -0.2$ similar to that in MACRO data. However, no significant deficit has been observed in the vertical bins. The Super-Kamiokande [1] with higher threshold than in MACRO and Baksan shows less profound Θ - effect, although some suppression of the flux is observed both at $\cos \Theta = -0.6 \div -0.2$ and in the vertical bins.

In [7] it was observed that oscillations of muon neutrinos to sterile neutrinos, $\nu_\mu \leftrightarrow \nu_s$, lead to the zenith angle dependence being qualitatively similar to that observed by MACRO experiment. In particular, it has been shown that the narrow dip in vertical bins can be due to the parametric enhancement of oscillations for neutrinos whose trajectories cross

both the mantle and the core of the Earth. The oscillation effect decreases with increase of the neutrino energy. This can explain absence of strong deficit in experiments with high thresholds like the Super-Kamiokande.

The $\nu_\mu \leftrightarrow \nu_s$ oscillations give as good description of the low energy (sub-GeV and multi-GeV) data as $\nu_\mu \leftrightarrow \nu_\tau$ do (see e.g. [8]). The appropriate region of oscillation parameters

$$\Delta m^2 = (2 \div 10) \cdot 10^{-3} \text{ eV}^2, \quad \sin^2 2\theta > 0.8 \quad (1)$$

is shifted slightly to larger values of Δm^2 in comparison with the $\nu_\mu \rightarrow \nu_\tau$ case due to matter effect which becomes important for $\nu_\mu \leftrightarrow \nu_s$ channel at small Δm^2 .

Crucial difference between $\nu_\mu \leftrightarrow \nu_s$ and $\nu_\mu \leftrightarrow \nu_\tau$ channels appears for high energy atmospheric neutrinos which are detected by upward-going muons. The matter effect is absent in $\nu_\mu \leftrightarrow \nu_\tau$ channel but it is important for $\nu_\mu \leftrightarrow \nu_s$ [9].

In this paper we perform a detailed study of the zenith angle dependences of the atmospheric neutrino and muon fluxes in presence of the $\nu_\mu \leftrightarrow \nu_s$ oscillations. We give a description of the parametric resonance effect in sect. 2. In sect. 3 we present results of calculations of the zenith angle dependences for the through-going and stopping muons. In sect. 4 we compare the prediction with experimental results.

2. Parametric resonance in atmospheric neutrinos

The $\nu_\mu \leftrightarrow \nu_s$ oscillations in matter are described by the 2×2 evolution matrix (the effective Hamiltonian) with off-diagonal elements $H_{\mu s} = H_{s\mu} = \Delta m^2/4E \cdot \sin 2\theta$ and the difference of the diagonal elements:

$$H_{\mu\mu} - H_{ss} = \frac{\Delta m^2}{2E} \cos 2\theta - V. \quad (2)$$

Here θ is the vacuum mixing angle, $\Delta m^2 \equiv m_2^2 - m_1^2$ is the mass squared difference (m_2 is the mass of the neutrino component which has larger admixture in ν_μ in the case of non-maximal mixing), E is the energy of neutrino and V is the matter potential

$$V = \frac{G_F}{\sqrt{2}} N_n, \quad (3)$$

where G_F is the Fermi constant, N_n is the neutron number density *. (For antineutrinos V has an opposite sign).

According to (2, 3) the length of $\nu_\mu \leftrightarrow \nu_s$ oscillations in matter and the effective mixing angle θ_m are determined by

$$l_m = \frac{2\pi}{V} [(\xi \cos 2\theta + 1)^2 + \xi^2 \sin^2 2\theta]^{-1/2}, \quad (4)$$

$$\sin^2 2\theta_m = \sin^2 2\theta \xi^2 [(\xi \cos 2\theta + 1)^2 + \xi^2 \sin^2 2\theta]^{-1}, \quad (5)$$

where

$$\xi = \frac{\Delta m^2}{2EV}. \quad (6)$$

In the case of maximal mixing the equations (4) and (5) are simplified:

$$l_m = \frac{2\pi}{V} [1 + \xi^2]^{-1/2}, \quad \sin^2 2\theta_m = \frac{\xi^2}{1 + \xi^2}.$$

For $\Delta m^2 > 4 \cdot 10^{-3} \text{ eV}^2$ both for the sub-GeV and multi-GeV ($E \sim 3 \div 5 \text{ GeV}$) events we get $\xi^2 > 10$ and the matter effect is small ($< 10\%$ in probability). Thus, in significant region of parameters (masses and mixing) at low energies the $\nu_\mu \leftrightarrow \nu_s$ oscillations reproduce results of the $\nu_\mu \leftrightarrow \nu_\tau$ oscillations, as far as the charged current interactions are concerned. (The number of the tau-lepton events is small.)

The matter effect becomes important for multi-GeV events if $\Delta m^2 < 3 \cdot 10^{-3} \text{ eV}^2$ [7,8]. In particular, the zenith angle dependence of ratios is modified. Since matter suppresses the $\nu_\mu \leftrightarrow \nu_s$ oscillations, one expects weaker oscillation effect for the upward-going neutrinos, and therefore, flatter zenith angle dependence than in the $\nu_\mu \leftrightarrow \nu_\tau$ case where matter effect is absent.

*Notice that in general case of ν_μ mixed with ν_τ and ν_e , the off-diagonal (mixing) elements get contributions from interaction with matter, and also the potential depends on electron/proton density.

The matter effect is important for distributions of the through-going and stopping muons [9] produced by high energy neutrinos even for large Δm^2 .

Let us first describe the zenith angle dependence of the survival probability $P(\nu_\mu \rightarrow \nu_\mu)$ for fixed neutrino energy. To a good approximation the Earth can be considered as consisting of the core and the mantle with constant densities and sharp change of density at the border between the mantle and the core. Therefore propagation of neutrinos through the Earth has a character of oscillations in layers with constant densities. This gives not only correct qualitative picture but also rather precise (as we will see) quantitative results.

According to (4) with increasing energy (decreasing Δm^2) $\xi \rightarrow 0$ and the oscillation length increases approaching the asymptotic value determined by the potential only: $l_m \approx 2\pi/V$. At the same time, the effective mixing angle decreases (5), so that the oscillation effects become weaker. Let us consider the range of energies which corresponds to $\xi = 0.1 \div 1$. Here l_m weakly depends on ξ , but $\sin^2 2\theta_m$ is not yet strongly suppressed. In this case the phase of oscillations, Φ , acquired by neutrino in a given layer ΔL equals:

$$\Phi = 2\pi \int^{\Delta L} \frac{dL}{l_m} \approx \int^{\Delta L} dL V . \quad (7)$$

The phase Φ depends on density and size of the layer, and it does not depend on neutrino energy. Using this feature we can immediately get the zenith angle dependence of $P(\nu_\mu \rightarrow \nu_\mu)$. Notice that for $\cos \Theta = -0.8$ neutrino trajectories touch the core of the Earth. Therefore for $\cos \Theta > -0.8$ neutrinos cross the mantle only, whereas for $\cos \Theta \lesssim -0.8$ they cross both the mantle and the core.

For $\cos \Theta \geq -0.8$ (mantle effect only), the survival probability can be written as

$$P \approx 1 - \sin^2 2\theta_m \sin^2 \frac{\Phi_m(\Theta)}{2}, \quad (8)$$

where the phase acquired by neutrinos, $\Phi_m(\Theta)$, equals:

$$\Phi_m(\Theta) \approx 2R_E |\cos \Theta| V \approx \sqrt{2} G_F N_n R_E |\cos \Theta| . \quad (9)$$

Here R_E is the radius of the Earth. From (9) we find $\Phi(\cos \Theta = -0.4) = \pi$, so that maximal

oscillation effect, $P_{max} = 1 - \sin^2 2\theta_m$, is at $\cos \Theta = -0.4$. At $\cos \Theta = -0.8$ the phase is $\Phi_m = 2\pi$, and the oscillation effect is zero.

For $\cos \Theta < -0.8$, neutrinos cross three layers: mantle, core and again mantle. The survival probability is $P = |S_{\mu\mu}|^2$, where the evolution matrix S equals

$$S = U(\theta_m)D(\Phi_m)U^+(\theta_m - \theta_c)D(\Phi_c)U(\theta_m - \theta_c)D(\Phi_m)U^+(\theta_m) . \quad (10)$$

Here $U(\theta_m)$ is the 2×2 mixing matrix, θ_m and θ_c are the mixing angles in matter of the mantle and core correspondingly. The matrix

$$D(\Phi) = \text{diag}(1, e^{i\Phi}) \quad (11)$$

describes the evolution of the eigenstates in certain layer; Φ_c and Φ_m are the phases of oscillations acquired in the core and in each layer of the mantle. It turns out that $\Phi_m \approx \pi$. Moreover, for $\cos \Theta \approx -0.88$ also Φ_c equals π . Thus for $\cos \Theta \approx -0.88$ we get the equality:

$$\Phi_{m1} \approx \Phi_c \approx \Phi_{m2} \approx \pi . \quad (12)$$

Under this condition an enhancement of oscillations occurs. Indeed, now $D = \text{diag}(1, -1)$ for all layers, and inserting this D in (10), we get the probability

$$P = |S_{\mu\mu}|^2 = 1 - \sin^2(4\theta_m - 2\theta_c). \quad (13)$$

Clearly for $\theta_c < \theta_m$, the probability P is smaller than $1 - \sin^2 2\theta_m$ and $1 - \sin^2 2\theta_c$ corresponding to maximal oscillation effect in one density layer. Moreover, the smaller θ_c (the stronger suppression of mixing in the core) the bigger the transition effect.

The condition (12) means that the size of the layer, R , coincides with half of the oscillation length: $R = l_m/2$. This is the condition of the parametric resonance [10,11] which can be written in general as, $2\pi \int_0^{r_f} dr/l_m = 2\pi k$, $k = 1, 2, 3, \dots$, where r_f is the size (period) of perturbation, and in our case $r_f = R_c + R_m$. Graphical representation [11] of the enhancement is shown in fig. 1: Mixing angle changes suddenly when the phase of system reaches π . This leads to increase of the oscillation angle. Thus one expects the (parametric

resonance) peak at $\cos \Theta = -0.88$. The width of the peak is $\Delta \cos \Theta \approx 0.12$. For exact vertical direction $\cos \Theta = -1$, we get $\Phi_c \approx 2.5\pi$ and the enhancement is destroyed. Thus unsuppressed flux is expected in this direction.

Let us stress that for sufficiently large energies the equality (12) does not depend on neutrino masses. The equality is determined basically by the density distribution in the Earth and by the potential which, in turn, is fixed by the channel of oscillations and the Standard Model interactions. The equality is fulfilled for oscillations into sterile neutrinos only. In the $\nu_\mu \leftrightarrow \nu_e$ channel the potential is two times larger and equality (12) is broken.

With the increase of the neutrino energy the form of the zenith angle dependence (position of minima and maxima) practically does not change, however the mixing angle, and therefore the depth of oscillations, diminish. Oscillation effect disappears for $\xi \ll 0.1$. In contrast, for low energies, $\xi \geq 1$, it reduces to the vacuum oscillations effect. Thus the profound zenith angle dependence with two dips exists in rather narrow range: $\xi \approx 0.1 \div 0.5$ (fig. 2). This dependence coincides qualitatively with the zenith angle dependence of the muon flux observed by the MACRO experiment. The Θ -distributions in fig. 2 have been calculated for real density profile of the Earth [12]. They close to the results obtained from (8) (10) for simplified model of the Earth (layers with constant density) (see fig.2 in [7]).

3. Zenith angle distribution of the upward-going muons

The flux of muons with energy above the threshold energy E_μ^{th} as a function of the zenith angle equals

$$F_\mu(E_\mu^{th}, \Theta) = \int_{E_\mu^{th}} dE \cdot \sum_{i=\nu, \bar{\nu}} F_i(E, \Theta) \cdot P_i(E, \Theta) \cdot Y_i(E, E_\mu^{th}), \quad (14)$$

where $F_\nu(E, \Theta)$ is the flux of original neutrinos, $P(E, \Theta)$ is the survival probability, and

$$Y_i(E, E_\mu^{th}) = \int_{E_\mu^{th}} R(E', E_\mu^{th}) \cdot \frac{d\sigma_i}{dE'}(E, E'_\mu) \quad (15)$$

is the probability that the neutrino with energy E produces muon, which arrives at a detector with the energy above E_μ^{th} . Here $R(E', E_\mu^{th})$ is the muon range (the distance in g/cm^2

at which muon energy decreases from E'_μ to E_μ^{th} due to energy loss) and $d\sigma/dE'_\mu$ is the differential cross section of $\nu_\mu N \rightarrow \mu X$ reaction.

The integrand in (14) at $P = 1$:

$$I = F(E, \Theta) \cdot Y(E, E_\mu^{th}) \quad (16)$$

describes the energy distribution of neutrinos that give rise to muon flux above E_μ^{th} . It has the form of a wide peak with full width on the half of height characterized by $1.5 \div 2$ orders of magnitude in E . This is substantially bigger than the width of region with significant two dips effect ($\xi = 0.1 \div 0.5$). A position of maximum of the peak, E_ν^{max} , depends on E_μ^{th} and Θ , and for $E_\mu^{th} \sim 1$ GeV one has $E_\nu^{max} \approx (20 \div 30)$ GeV.

Due to integration over neutrino energies the Θ - distribution of muons differs from the distribution of neutrinos shown in fig. 2. There are two modifications:

(i) Smoothing of Θ dependence occurs due to contributions from low energy neutrinos ($\xi \geq 1$) which undergo basically averaged vacuum oscillations effect. This leads to decrease of the peak between two dips in Θ -dependence.

(ii) Weakening of the overall suppression of the flux occurs due to contribution from high energy neutrinos with $\xi < 0.1$. For these neutrinos the oscillation effect is small due to smallness of mixing angle.

The dependence of the ratio of fluxes with and without oscillations F_μ/F_μ^0 on Θ for different values of Δm^2 is shown in fig. 3a. With increase of Δm^2 the region of strong oscillation effect ($P(E)$) shifts to higher energies and thus larger part of the neutrino spectrum will undergo suppression. This leads to overall strengthening of the oscillation effect, however the contribution from low energies also increases and the two dips zenith angle dependence becomes less profound. In contrast, for small Δm^2 the Θ -dependence is more profound, but overall suppression is weaker. Similar changes occur when the threshold, E_μ^{th} , varies (fig. 3b). With increase of E_μ^{th} (for fixed Δm^2) the peak of the integrand (16) shifts to higher energies; the Θ -dependence with two dips becomes more profound but overall suppression effect weakens. This can explain weaker effect in experiments with higher E_μ^{th} (like the

Super-Kamiokande). (Note that there is no $E_\mu^{th}/\Delta m^2$ scaling: the change of Δm^2 leads to stronger effect than similar change of $1/E_\mu^{th}$.)

For non-maximal mixing a dependence of the oscillation length on the neutrino energy becomes stronger: it appears in the lowest order in ξ . Indeed, from (4) we have

$$l_m \approx \frac{2\pi}{V} \frac{1}{1 \mp \xi \cdot \cos 2\theta} ,$$

where for $\Delta m^2 > 0$ minus and plus signs are for neutrinos and antineutrinos correspondingly. For non-maximal mixing the oscillation length of neutrinos is larger and the condition of the parametric resonance is fulfilled for larger $|\cos \Theta|$. Thus, the parametric peak shifts to vertical direction. For antineutrinos the length is smaller and the effect is opposite. Since the ν -flux is larger than $\bar{\nu}$ -flux the parametric peak for total flux shifts to larger $|\cos \Theta|$ (fig. 3c).

Uncertainties in the shape of the neutrino energy spectrum (and cross sections) can influence the zenith angle dependence. To study this effect we parameterize possible modifications of the spectrum, and consequently the integrand I as

$$I(E) = I_0(E) A E^{\alpha + \beta \ln(E/1\text{GeV})} , \quad (17)$$

where $I_0(E)$ is the integrand which corresponds to the spectrum from [13], α and β are parameters and A is a normalization factor. The results of the calculations for different values of parameters α and β are shown in fig. 3d. As follows from fig. 3, shift of the maximum to higher energies leads to suppression of the vacuum oscillation effect and therefore to more profound zenith angle dependence (dashed line), however the overall suppression becomes weaker. In contrast, the shift of the maximum to lower energies enhances the vacuum oscillation effect (dashed dotted line). Both more profound zenith angle dependence and strong overall suppression can be obtained for narrower $I(E)$ distribution (dotted line).

For stopping muon sample, the peak $I_{stop}(E)$ is narrow and its maximum is at smaller energies: $E \sim 10$ GeV. For $\Delta m^2 \geq 5 \cdot 10^{-3}$ eV² the matter effect is small ($\leq 10\%$), so that the zenith angle distribution is determined basically by vacuum oscillations (fig. 4).

Difference between $\nu_\mu \rightarrow \nu_s$ and $\nu_\mu \rightarrow \nu_\tau$ channels is small. For $\Delta m^2 \leq 4 \cdot 10^{-3} \text{ eV}^2$ the matter effect becomes important. The zenith angle dependence acquires the form with two dips.

Similarly, the sample of muons produced in the detector itself corresponds to low energies and narrow peak of the intergand, thus leading essentially to vacuum oscillations effect. So, we expect strong suppression of the number of these events which weakly depends on zenith angle.

4. Predictions versus experimental results

Let us compare the predicted distributions with the experimental results from the Baksan, MACRO (fig.5a) and Super-Kamiokande experiments (fig. 5 b). Histograms show the Θ -distribution averaged over the bins for “probe” point $\Delta m^2 = 8 \cdot 10^{-3} \text{ eV}^2$, $\sin^2 2\theta = 1$, and neutrino spectrum from [13]. The predicted suppression in the vertical bin is still weaker than in MACRO but stronger than in Baksan data. The predicted curve would fit better average of MACRO and Baksan results. Integrations over neutrino and muon energies result in strong smoothing of the distribution. The difference of suppressions in the dips and in the region between the dips is about $(15 \div 20) \%$. Without parametric effect one would expect the ratio $F_\mu/F_\mu^0 \rightarrow 1$ in the vertical bins. Notice that still error bars are large and the experimental situation for vertical bins is controversial (fig. 5a). In the same time there is a good agreement of predictions with the Super-Kamiokande zenith angle dependence (fig. 5b). Clearly, more data are needed to make any conclusion.

As follows from fig. 3, varying the neutrino parameters $(\Delta m^2, \sin^2 2\theta)$ and modifying neutrino spectrum one can change the predicted Θ -dependence. In particular, it is possible to make the dips move profound, to change relative depth of the dips, to shift positions of minima in $\cos \Theta$. Fitting the data one can also take into account uncertainties in normalization of original neutrino flux which can reach 20%.

Clearly Θ - dependences for $\nu_\mu \rightarrow \nu_s$ and $\nu_\mu \rightarrow \nu_\tau$ channels are different. The $\nu_\mu \rightarrow \nu_\tau$ oscillations lead to smooth enhancement of suppression with $|\cos \Theta|$, whereas the ν_μ

$\rightarrow \nu_s$ oscillations result in the structure with two dips. Furthermore, for vertical bins a suppression due to $\nu_\mu \rightarrow \nu_\tau$ is stronger than due to $\nu_\mu \rightarrow \nu_s$ and the difference can be as big as 20%. For $\nu_\mu \rightarrow \nu_\tau$ channel suppression weakly depends on the energy threshold, so that for Baksan/MACRO and Super-Kamiokande experiments the dependences are similar. In contrast, for $\nu_\mu \rightarrow \nu_s$ channel the suppression effect decreases with increase of the threshold. The effect is large for stopping muons (or muons produced in the detector), it is weaker for through-going muons in Baksan/MACRO and the weakest effect is for through-going muons in the Super-Kamiokande.

The two channels can be distinguished also by studying neutral current effects [14].

In conclusion, in the range of $\nu_\mu \rightarrow \nu_s$ oscillations parameters, which correspond to the best fit of the low energy data, the zenith angle dependence of the upward-going muons has a peculiar form with two dips at $\cos \Theta = (-0.6 \div -0.2)$ and $\cos \Theta = (-1.0 \div -0.8)$. The dip in vertical direction is due to parametric resonance in oscillations of neutrinos which cross the core of the Earth. This zenith angle dependence is crucial signature of a solution of the atmospheric neutrino problem, based on $\nu_\mu \leftrightarrow \nu_s$ oscillations.

Acknowledgments.

The authors are grateful to E. Kh. Akhmedov and P. Lipari for useful discussions. The work of Q.Y.L. is supported in part by the EEC grant ERBFMRXCT960090.

REFERENCES

- [1] Y.Totsuka (Super-Kamiokande Collaboration), in *LP'97*, 28th Int. Symposium on Lepton Photon Interactions, Hamburg, Germany, 1997, to appear in the Proceedings; E. Kearns, talk given at conference on *Solar Neutrinos : News About SNU's*, December 2-6, 1997, Santa Babara.
- [2] S.M. Kasahara et al., Phys. Rev. **D 55** (1997) 5282; T. Kafka, talk given at Fifth Int. Workshop TAUP-97, September 7 - 11, 1997, Gran Sasso, Italy.
- [3] Y. Fukuda et al., Phys. Lett. **B 335** (1994) 237.
- [4] R. Becker-Szendy et al., Phys. Rev. **D 46**, (1992) 3720; Nucl. Phys. B (Proc. Suppl.) **38** (1995) 331.
- [5] F. Ronga, Proceedings of the 17th International Conference on Neutrino Physics and Astrophysics (*Neutrino 96*), (1996) 529, edited by K. Enqvist, K. Huitu and J. Maalampi; T.Montaruli, talk given at TAUP 97, Sep. 1997 (Gran Sasso, Italy).
- [6] M.M. Boliev, et al., Proc. of the 8th “Rencontres de Blois” (*Neutrinos, dark matter and the universe*), edited by T. Stolarczyk, J. Tran Thanh Van, F. Vannucci (1996) 296.
- [7] Q. Y. Liu and A. Yu. Smirnov, hep-ph/9712493.
- [8] R. Foot, R.R. Volkas, O. Yasuda, TMUP-HEL-9801, (hep-ph/9801431); TMUP-HEL-9803, (hep-ph/9802287).
- [9] E. Akhmedov, P. Lipari, M. Lusignoli, Phys. Lett. **B 300** (1993) 128.
- [10] V.K. Ermilova, V.A. Tsarev and V.A. Chechin, Kr. Soob, Fiz. Lebedev Institute 5 (1986) 26; E. Akhmedov, Yad. Fiz. **47** (1988) 475 (Sov. J. Nucl. Phys. **47** (1988) 301).
- [11] P. I. Krastev and A. Yu. Smirnov, Phys. Lett. **B 226** (1989) 341.

- [12] see *e.g.* F. D. Stacey, *Physics of the Earth* (John Wiley and Sons, New York, 2nd edition, 1977.
- [13] V.Agrawal et al., Phys. Rev. D**53** (1996) 1314.
- [14] F. Vissani and A.Yu. Smirnov, hep-ph/9710565.

Figure Captions

Fig. 1. Graphical representation of the parametric enhancement of neutrino oscillations. Vector $\vec{\nu}$ describes the neutrino state in such a way that its projection on the axis Y gives $2P - 1$, where P is the probability to find ν_μ -neutrino. (The axis X is $\text{Re}(\psi_\mu^* \psi_s)$, where ψ_μ and ψ_s are the wave functions of the muon and sterile neutrinos.) The positions of ν -vector 2 - 4 correspond to ν -states at the borders of mantle and the core.

Fig. 2. The zenith angle dependence of the survival probability $P(\nu_\mu \rightarrow \nu_\mu)$ for different neutrino energies: solid line - 100 GeV, dashed line - 50 GeV, dash-dotted line - 30 GeV ($\Delta m^2 = 8 \cdot 10^{-3} \text{ eV}^2$).

Fig. 3. The zenith angle dependence of the ratio F_μ/F_μ^0 for the upward-going muons. a). the Θ dependences for different values of Δm^2 ($\sin^2 2\theta = 1$ and $E_\mu^{th} = 1 \text{ GeV}$); b). the same for different energy thresholds of muon detection, E_μ^{th} ($\sin^2 2\theta = 1$ and $\Delta m^2 = 8 \cdot 10^{-3} \text{ eV}^2$); c). the same for different values of mixing angle ($\Delta m^2 = 8 \cdot 10^{-3} \text{ eV}^2$ and $E_\mu^{th} = 1 \text{ GeV}$); d). the same for different original spectra of neutrinos described by parameters α, β in (17): $\alpha = 0.75, \beta = -0.075$ (dashed line) $\alpha = 0.25, \beta = -0.075$ (dash-dotted line) $\alpha = 0.75, \beta = -0.10$ (dotted line), solid line corresponds to unmodified neutrino flux.

Fig. 4. The zenith angle dependence of the ratio F_μ/F_μ^0 for stopping muons for different values of Δm^2 ($\sin^2 2\theta = 1$ and $E_\mu^{th} = 1 \text{ GeV}$).

Fig. 5. Comparison of the predicted zenith angle dependence (histograms) with experimental data from the MACRO and Baksan (a) and Super-Kamiokande ($E_\mu^{th} = 7 \text{ GeV}$) (b) experiments. Solid lines for $\nu_\mu \rightarrow \nu_s$ oscillations with $\Delta m^2 = 8 \cdot 10^{-3} \text{ eV}^2$ and $\sin^2 2\theta = 1$; dashed line for $\nu_\mu \rightarrow \nu_\tau$ oscillations with $\Delta m^2 = 5 \cdot 10^{-3} \text{ eV}^2$ and $\sin^2 2\theta = 1$.

FIGURES

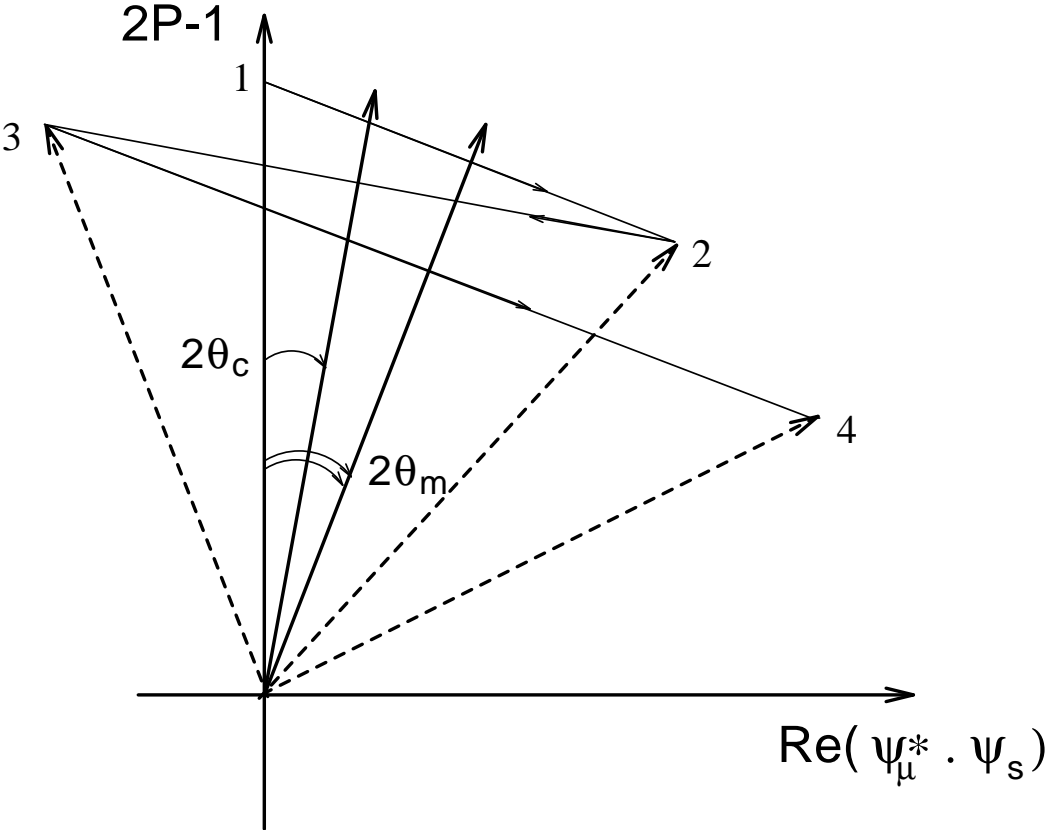


FIG. 1.

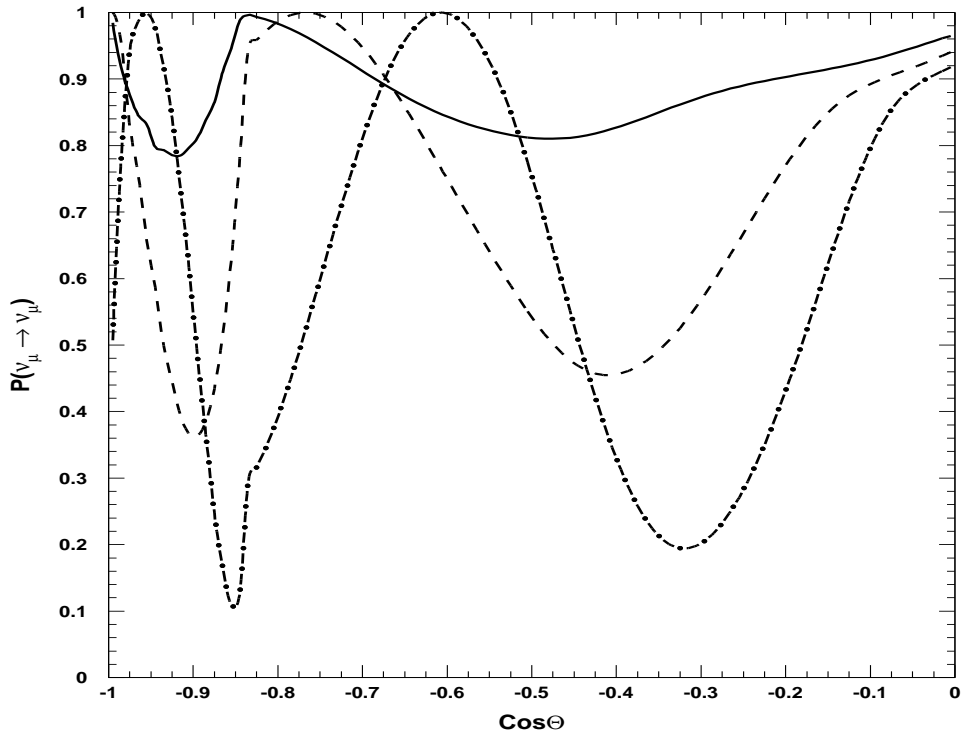
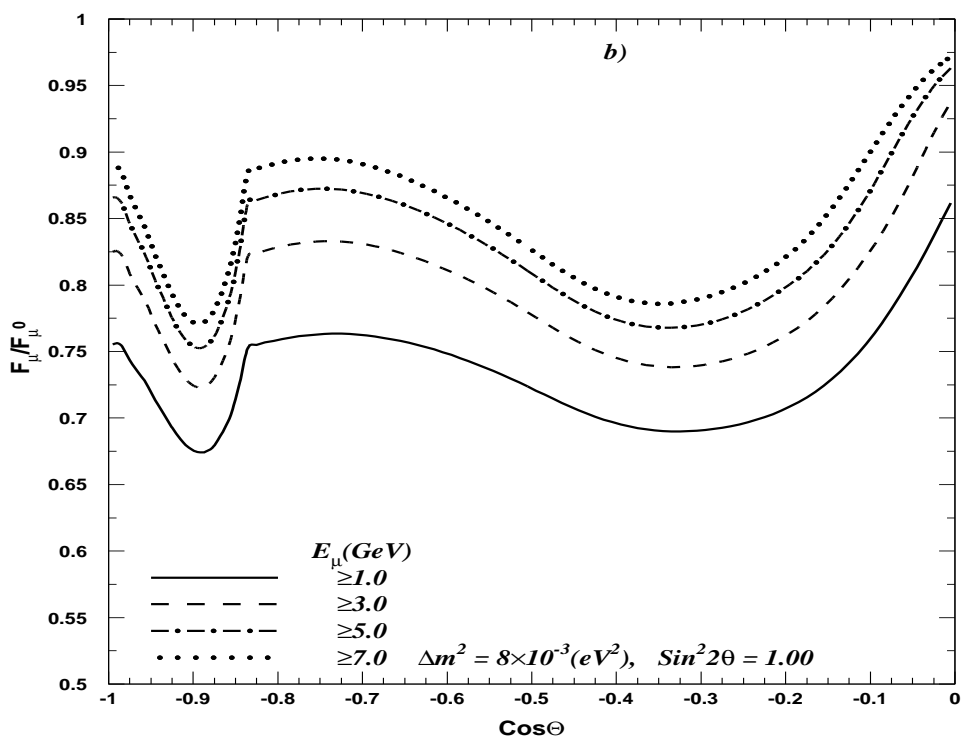
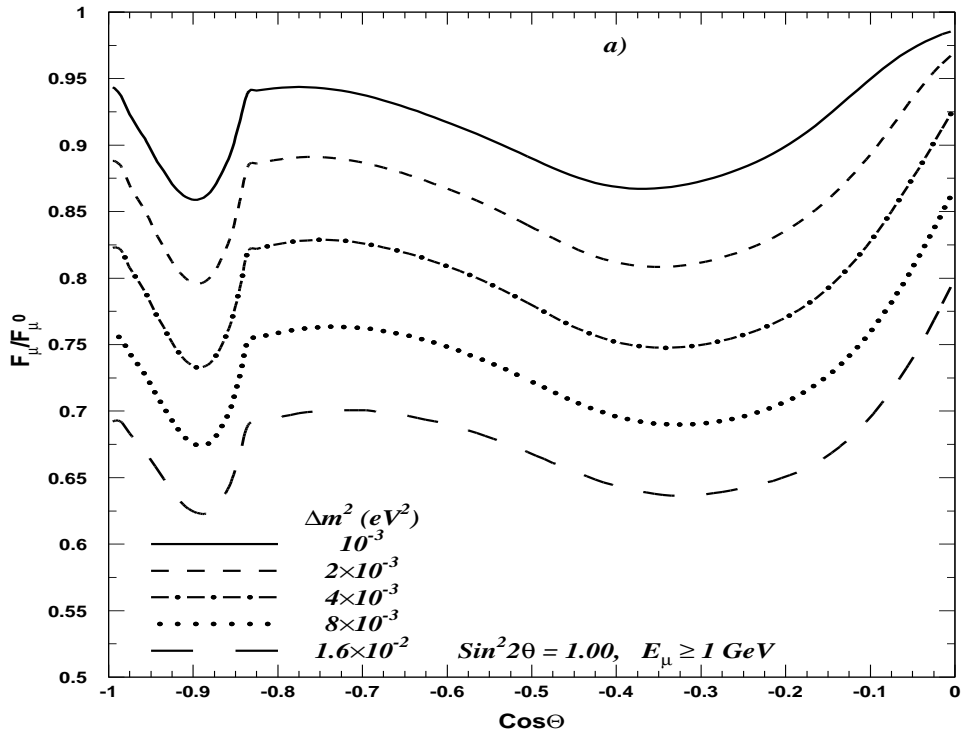


FIG. 2.



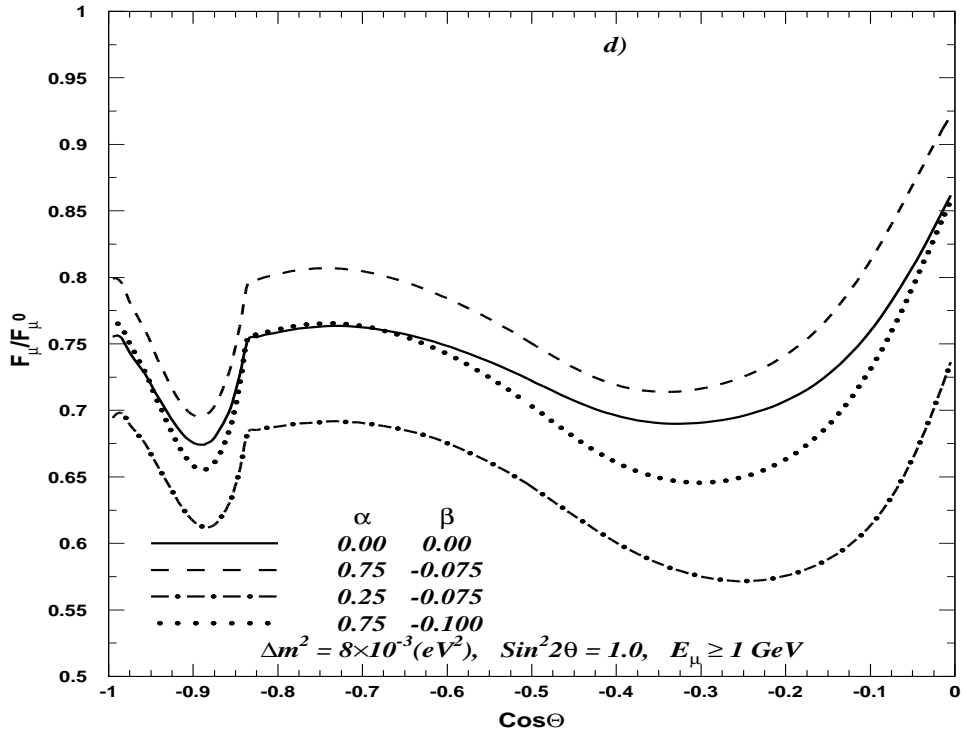
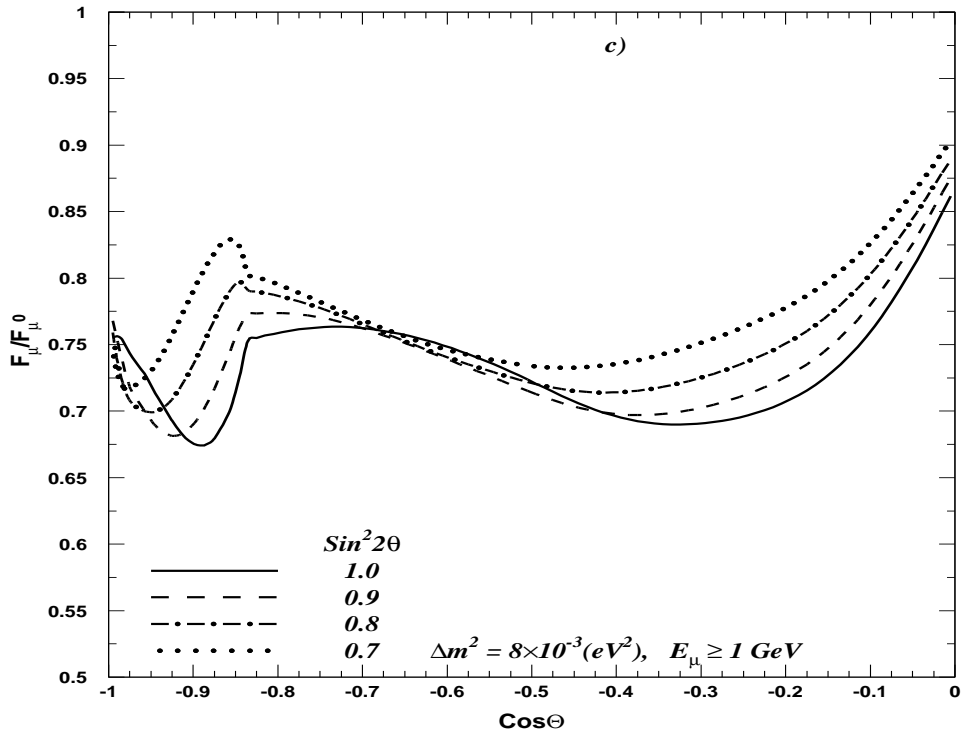


FIG. 3.

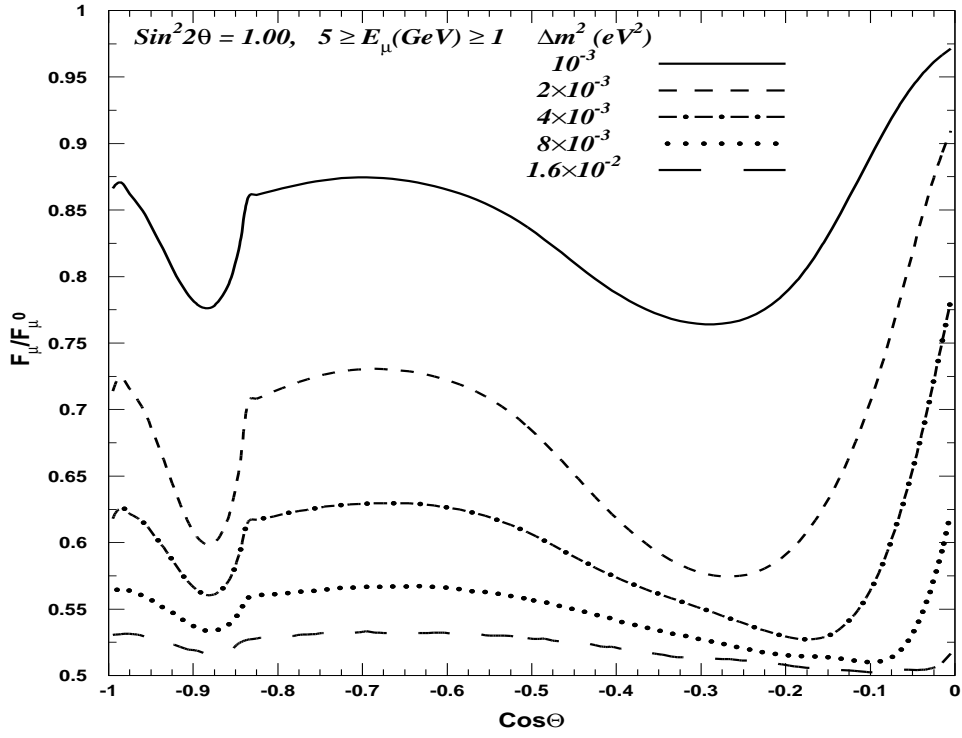


FIG. 4.

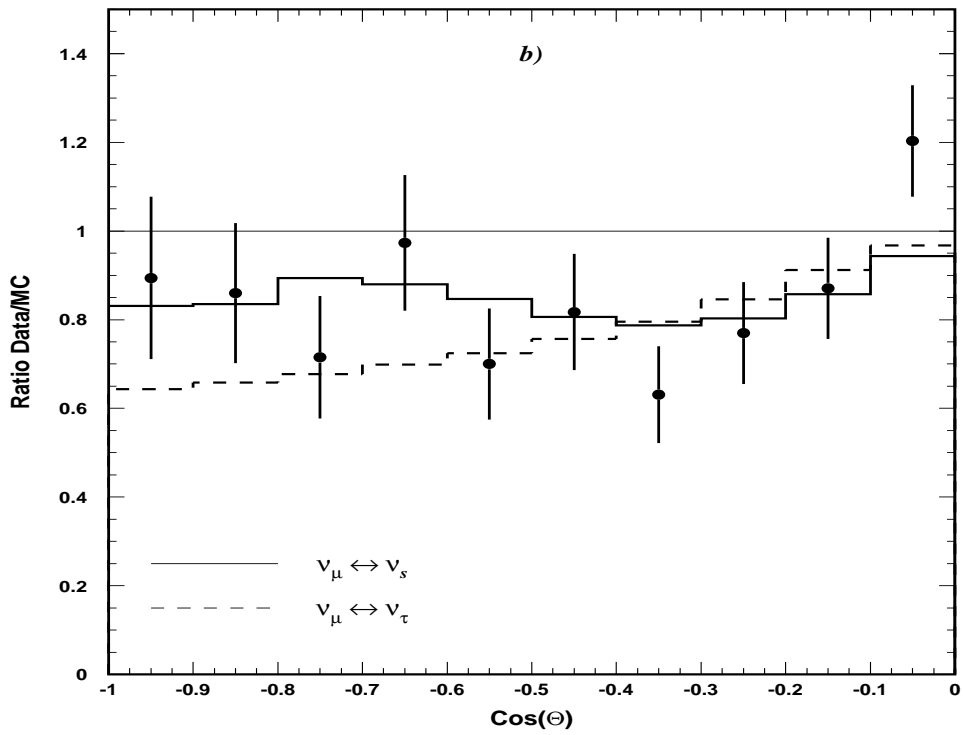
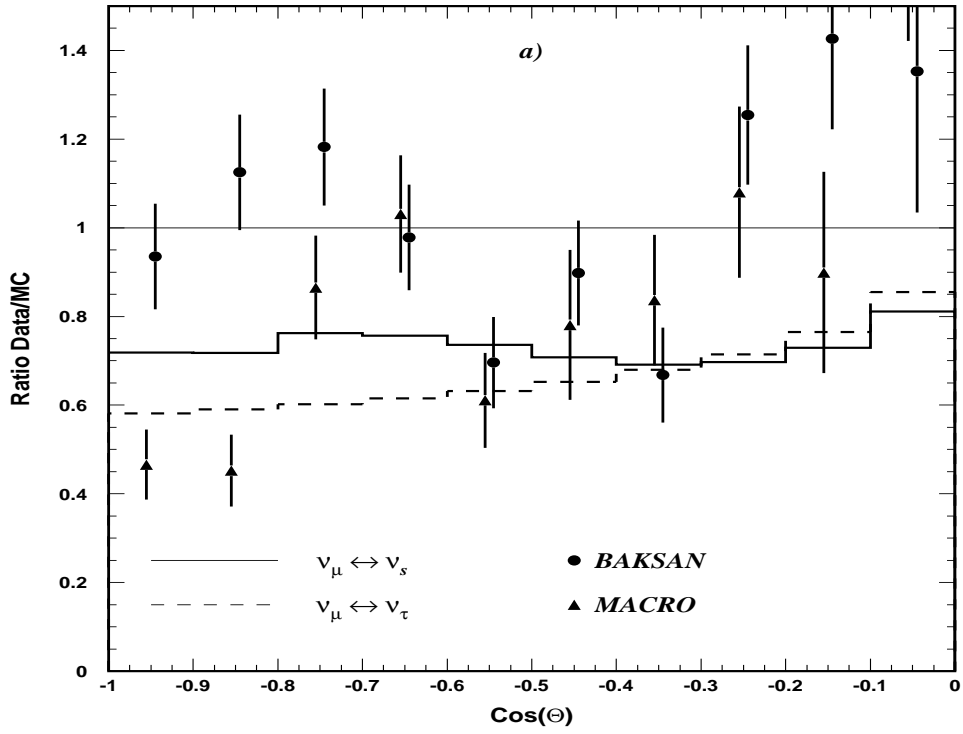


FIG. 5.